Chinese Chemical Letters 35 (2024) 108904

Contents lists available at ScienceDirect

Chinese Chemical Letters

journal homepage: www.elsevier.com/locate/cclet

Predesigned covalent organic framework with sulfur coordination: Anchoring Au nanoparticles for sensitive colorimetric detection of Hg(II)

Guorong Li, Yijing Wu, Chao Zhong, Yixin Yang, Zian Lin*

Ministry of Education Key Laboratory of Analytical Science for Food Safety and Biology, Fujian Provincial Key Laboratory of Analysis and Detection Technology for Food Safety, College of Chemistry, Fuzhou University, Fuzhou 350108, China

ARTICLE INFO

Article history:
Received 21 December 2022
Revised 31 July 2023
Accepted 6 August 2023
Available online 8 August 2023

Keywords:
Covalent organic frameworks
Thiazole
Sulfur coordination
Au nanoparticles
Hg^{2+}-activated peroxidase-like activity

ABSTRACT

Targeted construction of new covalent organic frameworks (COFs) with specific purposes and rationalities to build colorimetric assay platform for environmental pollutant monitoring have attracted increasing interest. However, it is still challenging due to lack of available coordination sites inside COFs pores and only a slight bonding ability for anchoring metal. In this work, a two-dimensional (2D) COFs (termed as Tz-COF) with high crystallinity, excellent chemical stability, and abundant sulfur coordination in its skeletons was synthesized and used for the confined growth of Au NPs. It was found that the Au NPs showed significant dispersibility for the support of Tz-COF. The proposed Tz-COF@Au NPs possessed outstanding Hg^{2+}-activated peroxidase-like activity benefited from physicochemical properties of gold amalgam and synergistic effect between COFs and Au NPs to oxidize chromogenic substrate. Based on highly efficient activity and distinctive color evolution, the strategy for detecting Hg^{2+} was developed and successfully applied to determine the content of Hg^{2+} in real environmental samples. This work manifests that a potential strategy to establish a colorimetric assay platform for environmental pollutant monitoring based on the targeted manufacturing of novel COFs with specific functions.

Metal nanoparticles (NPs) have attracted tremendous attentions due to unique optical, electronic, and mechanical properties, which have been extensively used in energy and biology [1]. Provided by high atomic utilization efficiency and catalytic performances, noble metal (Pt, Pd, Au, Ru, *etc.*) NPs are of particular attention for the applications in artificial enzymes [2,3]. Unfortunately, bare-metal NPs easily suffer from serious aggregation owing to their high surface energy, inevitably losing their catalytic performance. To address this challenge, various supporting substrates have been developed to load noble metal NPs to enhance their dispersibility, including carbon materials [4], porous silica [5], metal oxide [6,7] and metal organic frameworks (MOFs) [2].

Covalent organic frameworks (COFs), as an emerging class of crystalline porous materials, have achieved tremendous attention due to their structural periodicity, abundant porosity and functional diversity [8–10]. Compared with some traditional supports (*e.g.*, graphitic carbon nitride, MOFs), porous COFs not only have the highly pore channels which can be used to limit the growth of NPs [11,12], but also have good chemical stability in water, organic solvents, and even strong acidic or alkaline media [13–15]. For example, COFs were considered as carriers to upload active Au NPs [16]. The nanocomposite material with uniformly dispersed Au NPs in COFs exhibited outstanding catalytic performance [17–20]. Nevertheless, there is a lack of coordination environments of metal centers in COFs pore. It is challenging to regulate the chemical microenvironments of metal-COFs composites with specific purposes and rationalities.

Herein we performed the design of the newly targeted COFs with sulfur coordinated Au atoms, assigned as Tz-COF, by one-pot multicomponent method between thieno[3,2-*b*]thiophene-2,5-dicarboxaldehyde (TT), tetrakis(4-aminophenyl)ethane (ETTA), and elemental sulfur. The Tz-COF with regular heteroporous structure, large porosity, sufficient sulfur coordination as nucleation site for the *in situ* growth of Au NPs to form Tz-COF@Au NPs. The strong coordination interaction enabled the formation of fully-exposed Au NPs in Tz-COF. The Au NPs exhibited significant dispersibility. The as-prepared Tz-COF@Au NPs showed excellent Hg^{2+}-activated peroxidase-like activity by virtue of the physicochemical properties of gold amalgam and the synergistic effect of active Au NPs and COFs. Guided by this approach, the metal-COF composites with modular structures are regarded as sensing platforms coupled with

* Corresponding author.
E-mail address: zianlin@fzu.edu.cn (Z. Lin).

https://doi.org/10.1016/j.cclet.2023.108904
1001-8417/

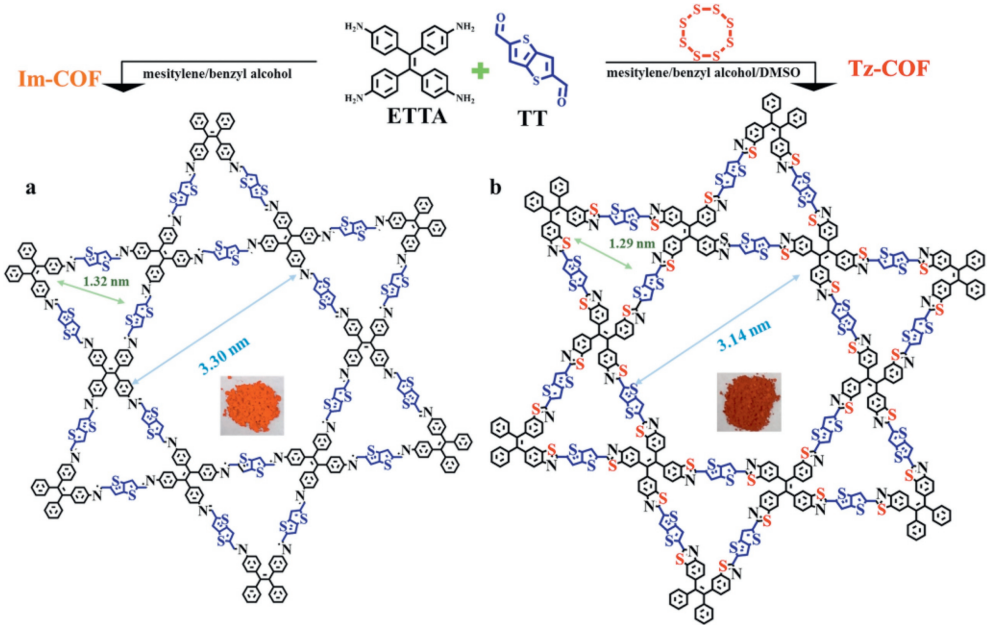

Fig. 1. Schematic illustration for the linker-exchange strategy. (a, b) Construction of heteroporous imine-linked COFs and thiazole-linked COFs *via* solvothermal method.

spectroscopic method and naked-eye for determination of Hg^{2+} levels in applications such as environmental monitoring.

The thiazole-linked COFs powders were obtained by three-component one-pot reaction between TT, ETTA, and elemental sulfur *via* a C–H functionalization and oxidative annulation [21] (Fig. 1 and Fig. S1 in Supporting information). To compare the Tz-COF, imine-linked COF (Im-COF) were obtained *via* a solvothermal method through the dehydration reaction between TT and ETTA [22]. Fourier-transform infrared (FT-IR) spectroscopy (Fig. S2 in Supporting information) showed a new peak at nearly 1607 cm^{-1} corresponding to the C=N of thiazole units. The peak at 1615 cm^{-1} corresponding to imine C=N stretch was disappeared [21,23]. Compared with Im-COF, Tz-COF were shifted positively by 0.67 eV at C 1s region in X-ray photoelectron spectroscopy (XPS) spectrum (Fig. S3 in Supporting information) owing to the interaction between sulfur and the carbon atom of the imine [21,24], which further confirmed the formation of a thiazole-bridged framework.

Scanning electron microscopy (SEM) revealed homogeneous morphologies for both COFs (Figs. 2a and b, and Figs. S4a and b in Supporting information), whereas the surface degree of Tz-COF was less rough. High-resolution transmission electron microscopy (HRTEM) images highlighted the crystallinity of both COFs due to their periodic porous structure (Fig. 2c and Fig. S4c in Supporting information). Straight hexagonal pores channels that extend through entire crystal domains were clearly visible. Both COFs showed similar lattice fringes of ~2.8 nm that was in good agreement with the simulated results. Furthermore, the bright diffraction spots and rings in fast Fourier transformation (FFT) patterns (the insets) showed a relatively hexagonal symmetry.

To evaluate the crystalline structure of both COFs, experimental and theoretical simulation were conducted. Tz-COF showed prominent diffraction peaks at 2.54°, 5.0°, 7.5°, 10°, 19.7°, which were indexed as (100), (200), (300), (400), and (001) reflections, respectively. Both the eclipsed stacking (AA) and staggered stacking (AB) models of hexagonal (H) and orthorhombic (O) geometrical structures for both COFs were simulated and investigated [25,26], we confirmed that their structure as hexagonal system with AA stacking (AA-H) were in good agreement with the experimentally acquired Powder X-ray Diffraction (PXRD) patterns (Figs. S5 and S6 in Supporting information). As shown in Fig. 2d and Fig. S4d (Supporting information), after Pawley refinement in space group P1, the optimized parameters were $a = b = 40.1995$ Å, $c = 4.4473$ Å, $R_{wp} = 11.22\%$, and $R_p = 7.53\%$ for Tz-COF ($a = b = 41.1994$ Å, $c = 4.5828$ Å, $R_{wp} = 10.06\%$, and $R_p = 7.04\%$ for Im-COF) [27], matched well with the eclipsed AA-H model (Tables S1 and S2 in Supporting information). Tz-COF exhibited the slight shift in the unit cell dimensions (Fig. S7 in Supporting information) [28]. Accordingly, both COFs had the expected architectures showing porous cavities. The pore channels showed that the abundant sulfur coordination in its hierarchical pores could provide potential recognition sites, which are favorable for supporting active Au NPs.

The porosities and pore size distributions of both COFs were examined using N_2 adsorption measurements at 77 K. As shown in Fig. 2e and Fig. S4e (Supporting information), reversible sorption curves exhibiting a combination of type I and type IV adsorption isotherms were observed for both COFs, which were typical feature of micropores and mesopores, respectively [25]. The calculated Brunauer-Emmett-Teller (BET) surface areas were 1459.7 and 1561.5 m^2/g for Tz-COF and Im-COF, respectively. The pore size distribution calculated by fitting the nonlocal density functional theory (NLDFT) were 1.27 and 3.09 nm in Tz-COF (Fig. 2f) and 1.31 and 3.1 nm in Im-COF (Fig. S4f in Supporting information). These values were agreement with the AA-H stacking structural model. With thiazole bridges throughout the frameworks, the prepared thiazole-based COFs was expected to significantly improve structural robustness [28]. The chemical stability of both COFs was maintained by comparing PXRD analysis after 24 h treatment in organic solvent, acid (0.1 mol/L HCl), and alkali (10 mol/L NaOH). The difference between the stability of imine-based COFs and the thiazole-based COFs was most striking in the case of acidic conditions, where Tz-COF showed no signs of degradation while the corresponding Im-COF nearly was labile (Fig. S8 in Supporting information). In addition, thermal gravimetric analysis (TGA) revealed both COFs were stable up to 450 °C (Fig. S9 in Supporting information).

The obtained Tz-COF possessed high crystallinity and porosity, and displayed outstanding chemical stability. More importantly, abundant sulfur coordination sites (thiazole and thiophene) inside the COFs showed strong binding interactions for anchoring Au. In-

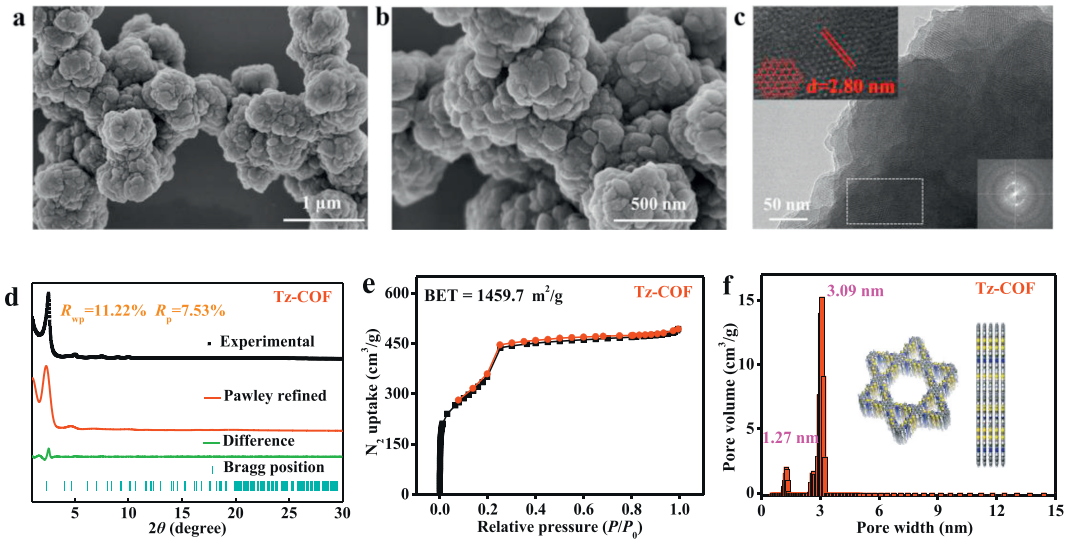

Fig. 2. (a, b) SEM images of Tz-COF. (c) HRTEM image of Tz-COF. Inset shows the corresponding FFT image. (d) Experimental and simulated PXRD patterns of Tz-COF. (e) N_2 sorption isotherms and (f) the corresponding pore width distribution of Tz-COF. Inset shows top and side views of the slipped AA stacking structures.

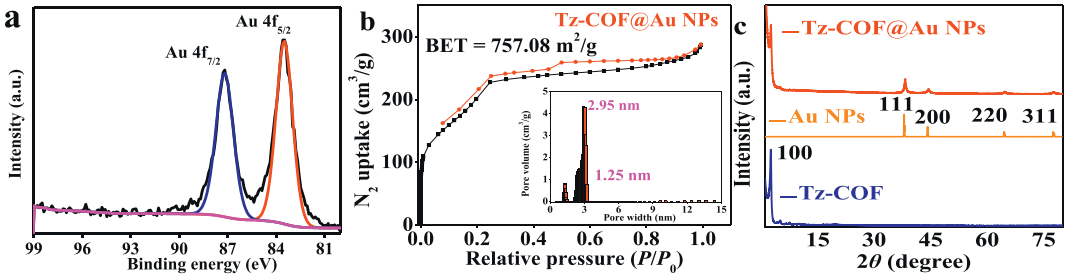

Fig. 3. (a) High-resolution spectra of Au 4f of Tz-COF@Au NPs. (b) N_2 adsorption isotherms of Tz-COF@Au NPs. Inset: the pore widths are centered at 1.25 and 2.95 nm, respectively. (c) Comparison of PXRD patterns of Tz-COF (blue), Au NPs (orange), and Tz-COF@Au NPs (red).

spired by these superiorities, Tz-COF could be used to induce nucleation for the *in situ* growth of Au NPs inside the accessible pores of COFs. First, adsorption energies were used to evaluate the adsorption strength of the relevant species on the both COFs. Au atom on active center (sulfur coordination environment) to form the adsorption species (Fig. S10 in Supporting information). The adsorption energies were listed in Table S3 (Supporting information). Tz-COF demonstrated a strong adsorption ability [29]. It had been proven that the existence of Au on the sulfur coordination was expected to form Tz-COF@Au NPs. Tz-COF@Au NPs was simply prepared by the reduction. The Au precursor was adsorbed inside the accessible pores of Tz-COF by adding $HAuCl_4{\cdot}3H_2O$ aqueous solution into a dispersion of Tz-COF and continuous stirring. The appearance variation of solution from initial bright red to dark (Fig. S11 in Supporting information). The oxidation state of the encapsulated Au species after reduction was determined by XPS. As shown in Fig. 3a and Fig. S12 (Supporting information), two characteristic peaks in the high-resolution Au 4f XPS spectrum with binding energies of 83.5 eV and 87.2 eV corresponding to Au $4f_{7/2}$ and Au $4f_{5/2}$ of Au^0 were observed, showing that Au NPs existed in the form of a metallic state (Au^0) [18]. The difference in porosity before and after Au loading was further supported by N_2 adsorption measurements. Fig. 3b indicated the decrease in the surface areas of Tz-COF@Au NPs (757.08 m^2/g) with respect to pristine COFs and the average size were found to be 1.25 and 2.95 nm, suggesting that Au NPs was bigger than the pore size of the COFs and distributed around the surface and the interlayer spacing of the COFs [19]. As shown in Fig. 3c, the PXRD of Tz-COF@Au NPs had the characteristics low angle peaks of the COFs and additional peaks at higher (2θ) values of 38.5°, 44.7°, 64.8°, and 77.7° corresponding to (111), (200), (220), and (311) reflections of metallic Au [30]. Additionally, TGA indicated a small residue amount after 1000 °C (Fig. S13 in Supporting information), revealing the successful loading of Au NPs into the pristine Tz-COF.

The HRTEM images (Fig. 4a) showed the highly dispersed Au NPs on the COFs material. Fig. 4b indicated that those Au NPs had interplanar spacing of 0.24 nm and 0.21 nm, assignable to the Au (111) and (200) planes, respectively. The corresponding selected area electron diffraction (SAED) pattern (Fig. 4c) was used to identify the polycrystalline feature of Au NPs and typical diffraction rings at (111), which was in good agreement with the PXRD pattern of Tz-COF@Au NPs. Some brighter white points could be obtained for Tz-COF@Au NPs in high-angle annular dark-field (HAADF) STEM (Fig. 4d). Corresponding EDS elemental mapping images (Figs. 4e-i) demonstrated highly homogeneous distributions. And the Tz-COF@Au NPs contained 13 wt% Au NPs (Fig. S14 in Supporting information). SEM images clearly revealed Au NPs were dispersed uniformly in the entire frameworks (Figs. 4j and k). Au NPs could generate *in situ* within the COFs. The strong interaction between the feasible coordination environment and Au enabled the formation of fully-exposed Au NPs on the hierarchical pore surface of Tz-COF [14]. The above results indicated the successful synthesis of Tz-COF@Au NPs *via in situ* growth of Au NPs that not only prevented from aggregation of Au NPs but also maintained the structural integrity of Tz-COF.

The typical colorimetric reactions, in which catalytic oxidation of 3,3′,5,5′-tetramethylbenzidine (TMB) to generate oxidized TMB (oxTMB) with blue color by H_2O_2 in presence of Tz-COF@Au NPs

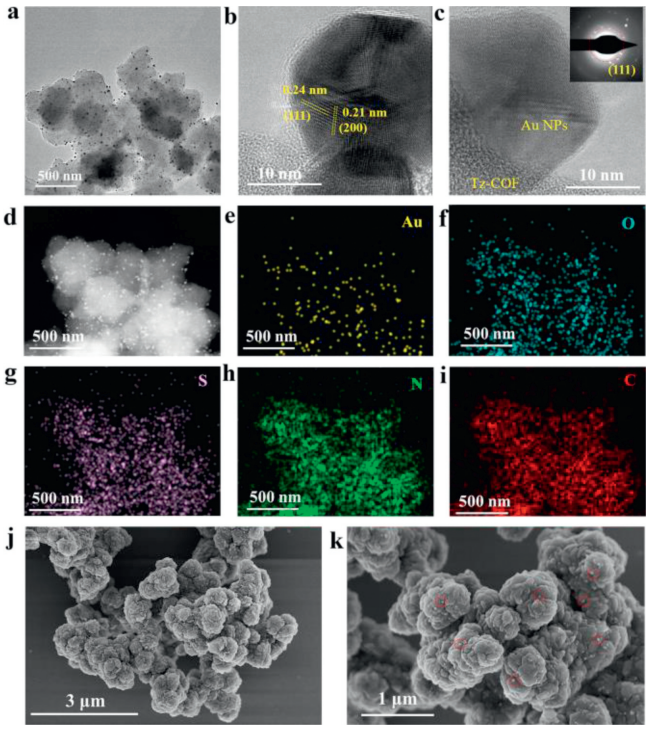

Fig. 4. (a) TEM analysis of Tz-COF@Au NPs. (b, c) The prominent lattice planes of Au NPs. Inset: SAED pattern in (c). (d) HAADF-STEM of Tz-COF@Au NPs. (e-i) Elemental mapping of selected areas in (d). (j, k) SEM image of Tz-COF@Au NPs. Scale bar, 3 μm and 1 μm.

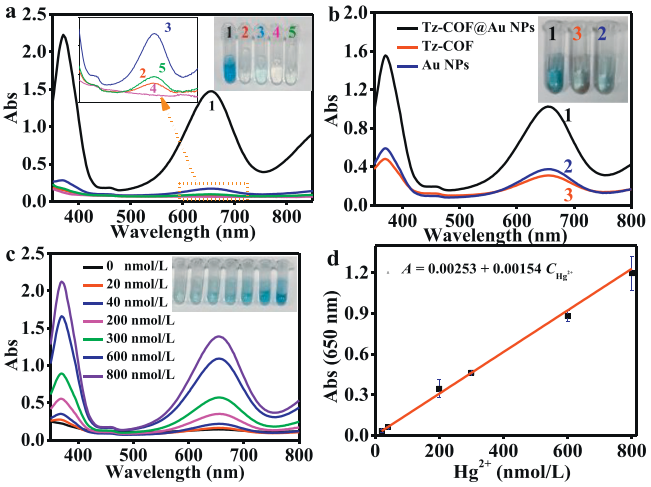

Fig. 5. (a) UV–vis absorption spectra of (1) Tz-COF@Au NPs + Hg^{2+} + H_2O_2 + TMB, (2) Tz-COF@Au NPs + H_2O_2 + TMB, (3) Hg^{2+} + H_2O_2 + TMB, (4) Tz-COF@Au NPs + Hg^{2+} + H_2O_2, and (5) Tz-COF@Au NPs + Hg^{2+} + TMB. The inset shows the corresponding color change. (b) Peroxidase-like activity of Tz-COF@Au NPs, Au NPs, and Tz-COF, (Tz-COF@Au NPs + TMB + H_2O_2; Tz-COF + TMB + H_2O_2; Au NPs + TMB + H_2O_2). The inset shows the color change of TMB. (c) UV–vis absorption spectra of Tz-COF@Au NPs with different amounts of Hg^{2+} in the TMB-H_2O_2 system. Inset: the photograph of the color changes. (d) Linear calibration curve for Hg^{2+} detection.

under a certain concentration of Hg^{2+}, were applied to evaluate the peroxidase-like activity. The result showed a strong UV–vis absorption peak at 650 nm (Curve 1 in Fig. 5a), indicating the Tz-COF@Au NPs exhibited prominent peroxidase mimetic activity in presence of Hg^{2+}. Compared with the control group without Hg^{2+}, Tz-COF@Au NPs, TMB, and H_2O_2, the blue product of oxTMB could not be formed (Curves 2, 3, 4 and 5 in Fig. 5a). The properties of peroxidase-like activity were dominated by the influence of Hg^{2+} uptake based on Au−Hg amalgam formation greatly changed the physicochemical properties [30–32]. Accordingly, H_2O_2 could be adsorbed on gold amalgam to form highly reactive hydroxyl radicals that oxidize TMB [33,34]. More importantly, Tz-COF@Au NPs showed a better peroxidase-like activity than Tz-COF and Au NPs due to the combined use of Tz-COF and Au NPs possessed excellent synergistic performance (Fig. 5b). In addition, the activity of Tz-COF@Au NPs could be adjusted according to the amount of $HAuCl_4$ (Fig. S15 in Supporting information). The result confirmed that the loading capacity of Au NPs into Tz-COF was limited and excessive agglomeration may impede enzyme-like activity of Tz-COF@Au NPs (Fig. S16 in Supporting information). In addition, to acquire excellent peroxidase-like activity, the effect of pH value, reaction time, TMB concentration, and Tz-COF@Au NPs concentration were optimized. As illustrated in Fig. S17 (Supporting information), the optimized experimental parameters to express the Hg^{2+}-activated peroxidase-like activity of Tz-COF@Au NPs were pH 4, 10 min, 30 mmol/L, and 3 mg/mL Tz-COF@Au NPs, respectively.

To the best of our knowledge, Hg^{2+} is a toxic metal ion in the environment, which will seriously damage the human health [35]. Therefore, the simple and sensitive detection of Hg^{2+} is of great significance. The prepared Tz-COF@Au NPs was good peroxidase-like nanocatalyst. Therefore, we had provided a colorimetric detection of Hg^{2+} based on the stimulus of intrinsic peroxidase-like catalytic activity of the Tz-COF@Au NPs. Fig. 5c illustrated the changes of the absorption spectra of the TMB + Tz-COF@Au NPs + Hg^{2+} system with different concentrations of Hg^{2+}. Fig. 5d showed the linear response of the assay at a low concentration of Hg^{2+} (20–800 nmol/L). The detection limit of the colorimetric assay was 11.3 nmol/L based on $3\sigma/k$, which was obviously lower than that of Hg^{2+} in the World Health Organization (WHO, 30 nmol/L) [31]. Compared with other analytical methods for Hg^{2+} detection (Table S4 in Supporting information), the colorimetric assay was more simple, and sensitive. To confirm the selectivity for the proposed Tz-COF@Au NPs toward toxic Hg^{2+}, we chose kinds of interfering ions including Ni^{2+}, Mg^{2+}, Ca^{2+}, Cd^{2+}, Al^{3+}, Pd^{2+}, Cr^{3+}, and Ag^{+}. As illustrated in Fig. S18 (Supporting information), the values were negligibly unchanged in the presence of some common metal ions. Thus, the results indicated that the present strategy possessed a high selectivity toward Hg^{2+}.

Mercury pollution caused by natural sources such as industrial waste, could exist for a long time. In general, Hg^{2+} was one of the most common forms of mercury pollution in aqueous solutions [36]. Water samples were collected. To explore the practicability of the sensing strategy, the standard addition approach was carried out to examine Hg^{2+} in water samples. The results were performed in Table S5 (Supporting information), the specific percent recovery of different concentrations of Hg^{2+} solution was calculated from 98.8% to 110.2% with the relative standard deviation (RSD) values ranging from 0.92% to 4.3%. It indicated that our proposed Tz-COF@Au NPs based colorimetric sensing platform was facile, feasible, and reliable in complex environments.

In conclusion, we have synthesized a Tz-COF with regular heteroporous structure, large porosity, abundant sulfur coordination in its skeletons as nucleation sites for Au NPs *in situ* growth, forming Tz-COF@Au NPs. The obtained Tz-COF@Au NPs showd a highly dispersed and stabilized Au NPs anchored in COFs with a high surface area. Tz-COF@Au NPs possessed outstanding Hg^{2+}-activated peroxidase-like activity due to physicochemical properties of gold amalgam and the synergistic effect of active Au NPs and COFs. A high-performance colorimetric detection platform for Hg^{2+} was developed. This sensing method exhibited satisfactory analytical performance in complex samples. This work not only provided a insight for monitoring Hg^{2+} pollutions conveniently but also a novel approach to create new and attractive COF-supported catalysts.

Declaration of competing interest

The authors declare that they have no known competing financial interests or relationships that could have appeared to influence the work reported in this paper.

Acknowledgments

This project was supported by the National Natural Science Foundation of China (Nos. 22274021, 21974021 and 22036001).

Supplementary materials

Supplementary data associated with this article can be found, in the online version, at doi:10.1016/j.cclet.2023.108904.

References

[1] C. Chen, D. Zhao, Y. Jiang, et al., Anal. Chem. 91 (2019) 15017–15024.
[2] Y. Huang, M. Zhao, S. Han, et al., Adv. Mater. 29 (2017) 1700102.
[3] R. Xu, Z. Wang, S. Liu, H. Li, Chin. Chem. Lett. 33 (2022) 4683–4686.
[4] X.K. Wan, H.B. Wu, B.Y. Guan, D. Luan, X.W.D. Lou, Adv. Mater. 32 (2020) 1901349.
[5] L. Shang, T. Bian, B. Zhang, et al., Angew. Chem. Int. Ed. 53 (2014) 250–254.
[6] W. Yuan, B. Zhu, K. Fang, et al., Science 371 (2021) 517–521.
[7] L. Duan, C.T. Hung, J. Wang, et al., Angew. Chem. Int. Ed. 61 (2022) e202211307.
[8] F. Jin, E. Lin, T. Wang, et al., Chemistry 8 (2022) 3064–3080.
[9] Z. Li, Z. Zhang, R. Nie, et al., Adv. Funct. Mater. 32 (2022) 2112553.
[10] L. Chen, M. Huang, B. Chen, et al., Chin. Chem. Lett. 33 (2022) 2867–2882.
[11] Q. Guan, L.L. Zhou, Y.B. Dong, Chem. Soc. Rev. 51 (2022) 6307–6416.
[12] Y. Zhang, G. Li, Y. Hu, Chin. Chem. Lett. 32 (2021) 2529–2533.
[13] H.C. Ma, J.L. Kan, G.J. Chen, C.X. Chen, Y.B. Dong, Chem. Mater. 29 (2017) 6518–6524.
[14] Y. Deng, Z. Zhang, P. Du, et al., Angew. Chem. Int. Ed. 59 (2020) 6082–6089.
[15] M. Yu, Y. Chen, M. Gao, et al., Small 19 (2022) 2206407.
[16] Y. Tian, Q. Lu, X. Guo, et al., Nanoscale 12 (2020) 7776–7781.
[17] R. Tao, X. Shen, Y. Hu, et al., Small 16 (2020) 1906005.
[18] L. Niu, X. Zhao, Z. Tang, et al., Sci. Total Environ. 835 (2022) 155423.
[19] X. Shi, Y. Yao, Y. Xu, et al., ACS Appl. Mater. Interfaces 9 (2017) 7481–7488.
[20] W. Ma, G. Li, C. Zhong, et al., Chem. Commun. 57 (2021) 7362–7365.
[21] K. Wang, Z. Jia, Y. Bai, et al., J. Am. Chem. Soc. 142 (2020) 11131–11138.
[22] A.C. Jakowetz, T.F. Hinrichsen, L. Ascherl, et al., J. Am. Chem. Soc. 141 (2019) 11565–11571.
[23] Y. Xie, Y. Chen, X. Sun, Y. Wang, Y. Wang, Chin. Chem. Lett. 32 (2021) 2061–2065.
[24] S.B. Ren, X.L. Chen, P.X. Li, et al., J. Power Sources 461 (2020) 228145.
[25] J. Dong, X. Li, S.B. Peh, et al., Chem. Mater. 31 (2018) 146–160.
[26] N. Liu, L. Shi, X. Han, et al., Chin. Chem. Lett. 31 (2020) 386–390.
[27] Z. Zhang, C. Kang, S.B. Peh, et al., J. Am. Chem. Soc. 144 (2022) 14992–14996.
[28] F. Haase, E. Troschke, G. Savasci, et al., Nat. Commun. 9 (2018) 2600.
[29] Q. Peng, Z.Y. Wang, B.S. Sa, B. Wu, Z.M. Sun, ACS Appl. Mater. Interfaces 8 (2016) 13449–13457.
[30] W.R. Cui, C.R. Zhang, W. Jiang, et al., ACS Sustain. Chem. Eng. 7 (2019) 9408–9415.
[31] L. Tan, Y. Zhang, H. Qiang, et al., Sens. Actuat. B: Chem. 229 (2016) 686–691.
[32] L. Chen, J. Li, L. Chen, ACS Appl. Mater. Interfaces 6 (2014) 15897–15904.
[33] J. Xu, F. Sun, Q. Li, et al., Small 18 (2022) 2200525.
[34] L. Wang, F. Gao, A. Wang, et al., Adv. Mater. 32 (2020) 2005423.
[35] Y. Guo, Y. Tao, X. Ma, et al., Chem. Eng. J. 350 (2018) 120–130.
[36] S. Zhang, D. Zhang, X. Zhang, et al., Anal. Chem. 89 (2017) 3538–3544.